

Multistep autoregressive reconstruction of seismic records

Mostafa Naghizadeh¹ and Mauricio D. Sacchi¹

ABSTRACT

Linear prediction filters in the f - x domain are widely used to interpolate regularly sampled data. We study the problem of reconstructing irregularly missing data on a regular grid using linear prediction filters. We propose a two-stage algorithm. First, we reconstruct the unaliased part of the data spectrum using a Fourier method (minimum-weighted norm interpolation). Then, prediction filters for all the frequencies are extracted from the reconstructed low frequencies. The latter is implemented via a multistep autoregressive (MSAR) algorithm. Finally, these prediction filters are used to reconstruct the complete data in the f - x domain. The applicability of the proposed method is examined using synthetic and field data examples.

INTRODUCTION

Reconstruction of seismic data using statistical approaches is an ongoing research topic in exploration seismology. Although many methods are based on statistical estimation theory, they also utilize information from the physics of wave propagation by taking into account relevant a priori information and assumptions. Methods proposed by Spitz (1991), Porsani (1999), and Gulunay (2003) successfully address interpolating spatially aliased regularly sampled data. These methods utilize low-frequency information to recover high-frequency data components. Spitz (1991) proposed to compute prediction filters (autoregressive operators) from low frequencies to predict interpolated traces at high frequencies. This methodology is applicable only if the original seismic section is regularly sampled in space. Conversely, irregularly sampled data can be reconstructed using Fourier methods. In this case, the Fourier coefficients of the irregularly sampled data are retrieved by inverting the inverse Fourier operator with a band limiting (Duijndam et al., 1999) and/or a sparsity constraint (Sacchi et al., 1998; Liu and Sacchi, 2004; Zwartjes and Gisolf, 2006).

We introduce a new strategy that combines the strengths of both prediction-error methods and Fourier-based methods to cope with the problem of reconstructing nonuniformly sampled, aliased data. The first step of the proposed algorithm involves the reconstruction of irregularly missing spatial data on a regular grid at low frequencies using Fourier-based algorithms. Because of the band-limited nature of the wavenumber spectra at low frequencies, this portion of data can be reconstructed with high accuracy (Duijndam et al., 1999). Then using a multistep autoregressive (MSAR) algorithm, the prediction filters of all the frequencies are extracted from the reconstructed low-frequency portion of the data. These prediction filters are utilized to reconstruct the missing spatial samples of each frequency in the f - x domain.

It is important to stress that the technique presented in this paper can only be used to reconstruct data that live on a regular grid with missing observations. Zwartjes and Sacchi (2007) introduced a method that combines the f - k algorithm of Gulunay (2003) and Sparse inversion (Zwartjes and Gisolf, 2006) to reconstruct irregularly sampled aliased data. In their algorithm the nonuniform discrete Fourier transform (NDFT) is utilized to handle the irregularly sampled data.

THEORY

Problem statement

Consider a seismic gather containing linear events. In addition, we assume that some traces in the gather are missing. By applying the discrete Fourier transform (DFT) with respect to time, the gather is transformed to the f - x domain. We let $\mathbf{x}(f)$ be the length- N vector of f - x data sampled on a regular grid $x_1(f), x_2(f), x_3(f), \dots, x_N(f)$, of which only M traces are available. Let the sets of integers $\mathcal{K} = \{k(1), k(2), k(3), \dots, k(M)\}$ and $\mathcal{U} = \{u(1), u(2), u(3), \dots, u(N - M)\}$ indicate the indices of available (known traces) and missing samples (unknown traces), respectively. The goal is to recover $\mathbf{x}_l(f)$ from $\mathbf{x}_{\mathcal{K}}(f)$.

Manuscript received by the Editor 27 February 2007; revised manuscript received 11 May 2007; published online 5 September 2007.

¹University of Alberta, Department of Physics, Edmonton, Alberta, Canada. E-mail: mnaghizadeh@ualberta.ca; sacchi@ualberta.ca.
© 2007 Society of Exploration Geophysicists. All rights reserved.

Reconstruction of the unaliased part of the data using minimum-weighted norm interpolation

Fourier reconstruction methods are well suited to reconstruct seismic data in the low-frequency (unaliased) portion of the Fourier spectrum. In addition, as it was shown by Duijndam et al. (1999), the reconstruction problem is well-conditioned at low frequencies where only a few wavenumbers are required to honor the data. This makes the problem well-posed; therefore, it is quite easy to obtain a low-frequency spatial reconstruction of the data.

With the previous reasoning in mind, we first proceed to restore the low-frequency portion of the data using a Fourier reconstruction method. In other words, we estimate the missing samples of $\mathbf{x}(f)$, that is $\mathbf{x}_u(f)$ from $\mathbf{x}_k(f)$ for temporal frequencies $f \in [f_{\min}, f_{\max}]$, where f_{\min} and f_{\max} denote the minimum and maximum (unaliased) frequencies in the data. In general, because of the band-limited nature of the seismic wavelet, we consider $f_{\min} > 0$.

Recently, two Fourier-based reconstruction methods were introduced: band-limited Fourier reconstruction (BLFR) (Duijndam et al., 1999; Schonewille et al., 2003) and minimum-weighted norm interpolation (MWNI) (Liu and Sacchi, 2004; Liu et al., 2004; Sacchi and Liu, 2005). In our implementation, we have adopted MWNI. It is important to mention, however, that similar results were obtained using BLFR. These methods can retrieve the complex Fourier coefficients of the reconstructed data directly from the observations by inverting the inverse Fourier operator. The nonuniqueness of the reconstruction problem (Sacchi et al., 1998) is circumvented by the incorporation of a constraint in the form of a spectral norm. Details pertaining the MWNI method are discussed in Appendix A.

Estimation of prediction filters using MSAR

Let us consider reconstructed data in the band $f \in [f_{\min}, f_{\max}]$. In Appendix B we show that linear events in the f - x domain can be predicted using MSAR operators of the form,

$$x_n(f) = \sum_{j=1}^L P_j(\alpha f) x_{n-\alpha j}(f), \quad n = \alpha L + 1, \dots, N, \quad (1)$$

$$x_n^*(f) = \sum_{j=1}^L P_j(\alpha f) x_{n+\alpha j}^*(f), \quad n = 1, \dots, \alpha N - L, \quad (2)$$

where $*$ denotes complex conjugate. These equations correspond to a special type of autoregressive (AR) model where forward (equation 1) and backward (equation 2) AR equations are computed by jumping α steps at the time. The length of the AR operator is L and $P_j(f)$ is the prediction filter. The parameter $\alpha = 1, 2, \dots, \alpha_{\max}$ is the step factor used to extract the prediction filter for frequency αf from frequency f . Because the step factor is a positive integer, it is clear that low frequencies provide vital information for our data reconstruction algorithm.

The parameter α_{\max} is the upper limit of the step factor in equations 1 and 2. The latter depends on the number of traces N and the length of prediction filter L . This parameter is given by

$$\alpha_{\max} = \left\lfloor \frac{N - \frac{L+1}{2}}{L} \right\rfloor,$$

where $\lfloor \cdot \rfloor$ denotes the integer part.

Equations 1 and 2 can be considered an extension of the prediction filters used by Spitz (1991). In our case, however, multiple prediction filters are extracted for a given high frequency $f' = \alpha f$. In other words, all possible combinations of α and f leading to the product $f' = \alpha f$ will deliver a prediction filter that can be used to reconstruct data at frequency component f' . Because more than one prediction filter can be found for the reconstruction of $\mathbf{x}(f')$, our algorithm utilizes the average of prediction filters. Alternatively, we could have estimated one prediction filter by solving an augmented system of equations with contributions from more than one low frequency. The final result of both strategies should be quite similar. We have adopted the former rather than the latter because it leads to a computationally more efficient reconstruction algorithm.

To continue with our analysis, a few comments are in order. The MSAR strategy requires us to find prediction filters in the reconstructed band $[f_{\min}, f_{\max}]$ where \min and \max are discrete frequency indices. We might encounter the case where for some frequency f' , the frequency f'/α may not fall in the reconstructed interval $[f_{\min}, f_{\max}]$; and then, the MSAR method will not be applicable. This situation can be solved by extrapolating prediction filters using the method proposed in Appendix B of Spitz (1991). It should be mentioned that this situation can be avoided by properly choosing the values of f_{\min} and f_{\max} in such a way that $\max \geq 2(\min - 1)$. In the sections devoted to examples, we provide a synthetic test (Example 2) where the extrapolation of prediction filters is required to reconstruct aliased data.

Reconstruction of missing samples using prediction filters

So far, we have outlined a method to extract, from reconstructed low-frequency data components $\mathbf{x}(f)$, prediction filters for high-frequency data component $\mathbf{x}(f') = \mathbf{x}(\alpha f)$.

Following the procedure proposed by Wiggins and Miller (1972) and Spitz (1991), one can compute the missing samples from known data and prediction filter coefficients. In this case, the forward and backward autoregressive equations,

$$x_n(f') = \sum_{j=1}^L P_j(f') x_{n-j}(f'), \quad n = L + 1, \dots, N, \quad (3)$$

$$x_n(f') = \sum_{j=1}^L P_j^*(f') x_{n+j}(f'), \quad n = 1, \dots, N - L, \quad (4)$$

are used to isolate the unknown data components. Equations 3 and 4 are specific forms of equations 1 and 2 when $\alpha = 1$. It is also important to notice that equation 4 is obtained by taking complex conjugate of both sides of equation 2. Now both forward and backward prediction equations contain the same unknown $x(f')$. The rest of procedure is quite simple: We first expand equations 3 and 4. The resulting system of equation contains linear combinations of known and unknown samples. The system is algebraically manipulated and rewritten as follows:

$$\tilde{\mathbf{A}}(\mathbf{P}(f')) \begin{bmatrix} x_{u(1)}(f') \\ x_{u(2)}(f') \\ \vdots \\ x_{u(N-M)}(f') \end{bmatrix} = \tilde{\mathbf{B}}(\mathbf{P}(f')) \begin{bmatrix} x_{k(1)}(f') \\ x_{k(2)}(f') \\ \vdots \\ x_{k(M)}(f') \end{bmatrix}. \quad (5)$$

The notation $\tilde{\mathbf{A}}(\mathbf{P}(f'))$ and $\tilde{\mathbf{B}}(\mathbf{P}(f'))$ reflects the fact that these two matrices only depend on the coefficients of the prediction filter. Equation 5 closely follows equation 5 of Spitz (1991). However, the main difference is that the known and unknown traces are no longer interlaced, but are given at arbitrary positions. In addition, it is important to stress that $\mathbf{P}(f')$ is the average of prediction filters computed from reconstructed low frequencies using the MSAR scheme. Hence, the missing samples are computed using:

$$\mathbf{x}_\mathcal{U}(f') = [\tilde{\mathbf{A}}^*(\mathbf{P}(f')) \tilde{\mathbf{A}}(\mathbf{P}(f')) + \mu \mathbf{I}]^{-1} \times \tilde{\mathbf{A}}^*(\mathbf{P}(f')) \tilde{\mathbf{B}}(\mathbf{P}(f')) \mathbf{x}_\mathcal{K}(f'), \quad (6)$$

where $\mathbf{x}_\mathcal{U}(f')$ and $\mathbf{x}_\mathcal{K}(f')$ indicate the vectors of unknown and known data samples, respectively. In addition, $\tilde{\mathbf{A}}^*$ stands for the transpose and complex conjugate of $\tilde{\mathbf{A}}$, \mathbf{I} is the identity matrix, and μ is a regularization parameter required to stabilize the inversion in the presence of noise. In this paper, the conjugate gradient method is used to solve equation 5.

DATA EXAMPLES

Example 1

To examine the performance of the MSAR reconstruction technique, we analyze two synthetic-data examples. Amplitude spectra

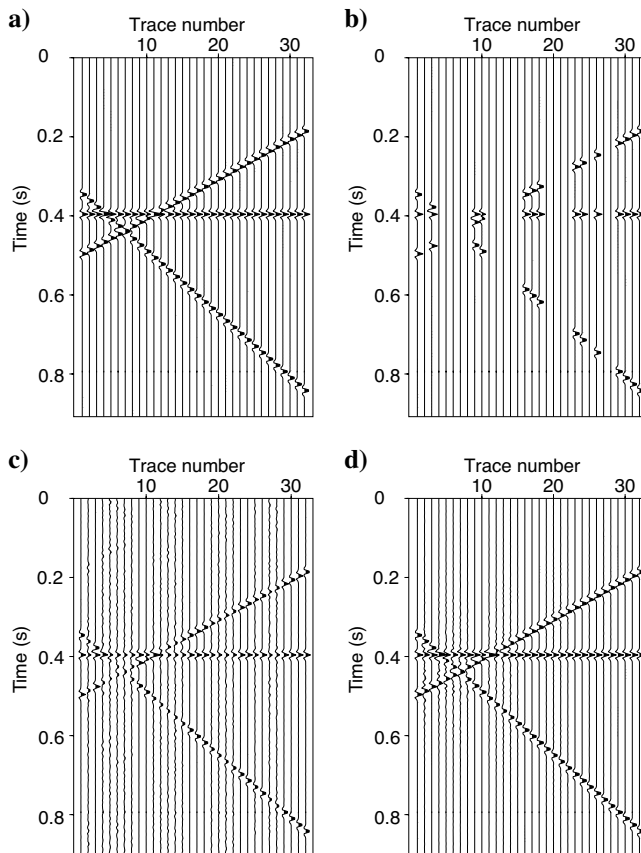


Figure 1. Synthetic example in t - x domain. (a) Original data. (b) The data with missing traces. (c) Reconstructed section using MWNI. (d) Reconstructed section using MWNI and MSAR. Notice that MWNI was used to reconstruct data in the normalized frequency band $0.035 - 0.075$. The remaining part of the band ($0.075 - 0.5$) was reconstructed via MSAR.

are portrayed in terms of normalized frequency and normalized wavenumber. Normalized frequency and wavenumber axes are obtained by considering $\Delta t = 1$ and $\Delta x = 1$, respectively. This means that to obtain frequency axes in Hertz and Cycles/m, one must divide the normalized ones by Δt and Δx , respectively.

The first synthetic data consist of three linear events. Two of them are severely aliased. In addition, we have randomly removed 60% of the traces. Figure 1a and b show the original complete data and the data with missing traces, respectively. The data with missing traces were reconstructed using the MWNI method for normalized frequencies in a range of 0.035 to 0.5. The result is portrayed in Figure 1c. In addition, we have used MWNI to reconstruct only the low-frequency portion of the data from normalized frequencies in the 0.035 to 0.075 range. After extracting prediction filters from low-frequency data components, the complete data spectrum was reconstructed with the MSAR technique (for normalized frequencies in the range 0 to 0.5). The length of the prediction filter is chosen equal to the number of linear events ($L = 3$). The final result is provided in Figure 1d. Both methods were capable of reconstructing the data. However, the high frequencies were better restored via the combined application of MWNI and MSAR. This is emphasized by Figures 2 and 3 where we show the f - k and f - x panels of the data portrayed in Figure 1. In particular, one observes that all the high-frequency artifacts generated by MWNI (Figure 2b) were attenuated (Figure 2d).

For completeness, Figure 4a and b show the normalized low-frequency band in the 0.035 to 0.075 range reconstructed via MWNI. We must reiterate that this is the portion of reconstructed data from

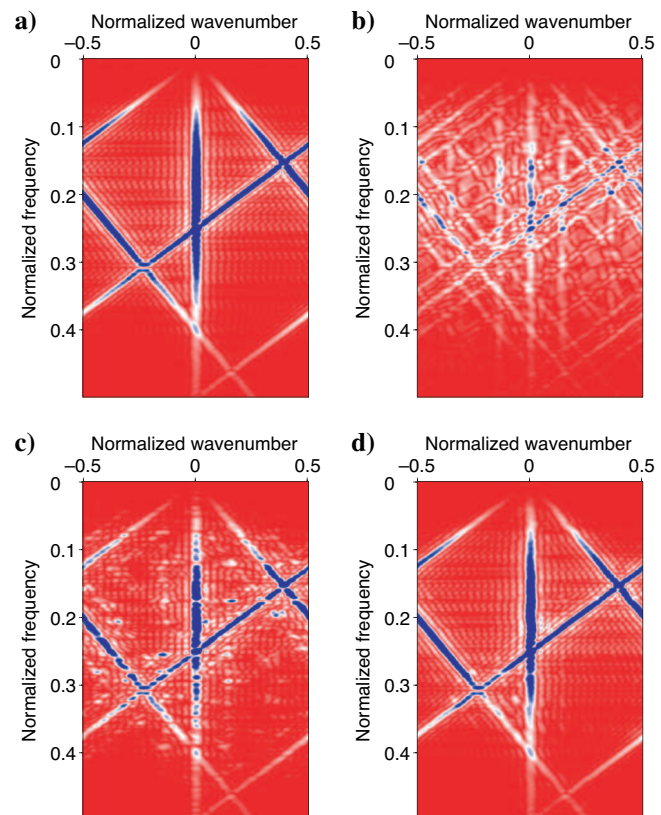


Figure 2. The f - k representation of Figure 1. (a) Original data. (b) Data with missing traces. (c) Reconstructed data via MWNI. (d) Reconstructed data via MWNI and MSAR.

where the MSAR technique will extract the prediction filters needed to reconstruct high-frequency components. Figure 5 shows the number of prediction filters extracted for each frequency using the MSAR method. Because of the lack of information, the very low frequencies were excluded from the reconstruction. Prediction filters for the low-frequency end of the data could have been estimated by extrapolation of prediction filters as suggested in Spitz, 1991 Appendix B.

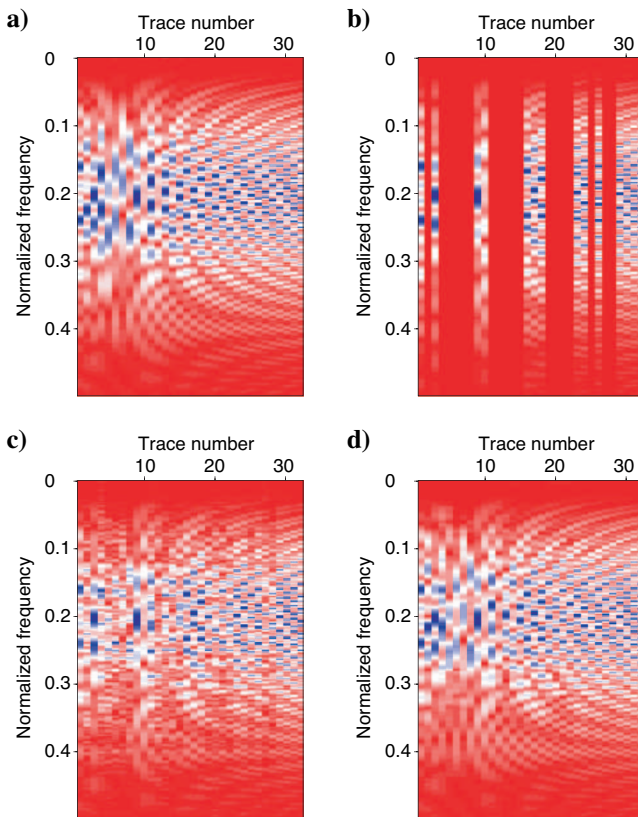


Figure 3. The f - x representations of Figures 1. (a) Original data. (b) Data with missing traces. (c) Reconstructed data via MWNI. (d) Reconstructed data via MWNI and MSAR.

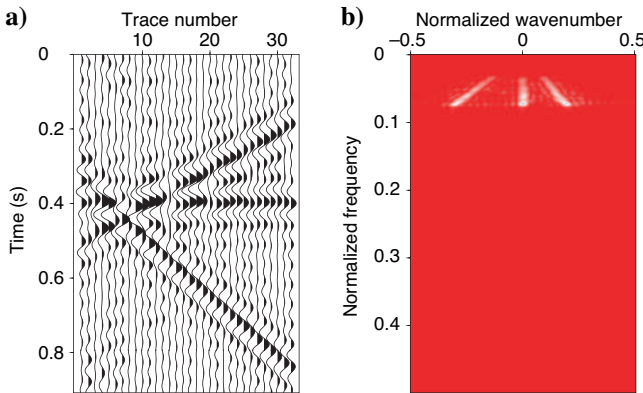


Figure 4. Reconstructed low-frequency portion of the data using MWNI. Prediction filters required to reconstruct high-frequency data components were extracted from this data set (Figure 1d). (a) t - x domain. (b) f - k domain.

Example 2

To continue testing our algorithm, we provide a second example (Figure 6) where MWNI was used to reconstruct the normalized frequencies in the 0.07 to 0.084 range (Figure 6b and e). We have chosen this particular frequency band to simulate a situation where MSAR will fail in finding enough prediction filters to reconstruct the data. Figure 7 shows the number of prediction filters computed using MSAR for each frequency. The gaps in Figure 7 belong to the frequencies for which the MSAR scheme was not able to find a prediction filter. For a frequency component f' falling within a gap, the corresponding low-frequency component f'/α falls out of the interval $[f_{min}, f_{max}]$; therefore, there is no way of extracting prediction filters for those frequencies. As we have already mentioned, these missing prediction filters can be estimated using extrapolation methods. In this case, the known prediction filters can be used to find the prediction filters in the gaps using the method provided in Appendix B of Spitz (1991).

In summary, by using MSAR plus extrapolation of prediction filters, we have been able to retrieve all the information necessary to reconstruct the data for all the frequencies. The results are shown in Figure 6a-d. The result is quite good considering that the prediction filters in the four gaps in Figure 7 were computed using estimated prediction filters followed by extrapolation. The situation described

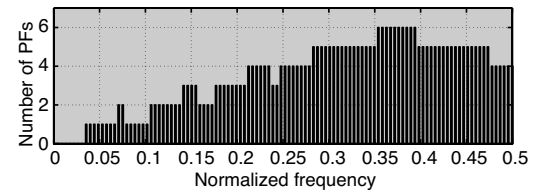


Figure 5. The number of prediction filters contributing to each frequency components in the example in Figure 1d. The average filter for any given frequency is used in the reconstruction stage of the algorithm (equation 6).

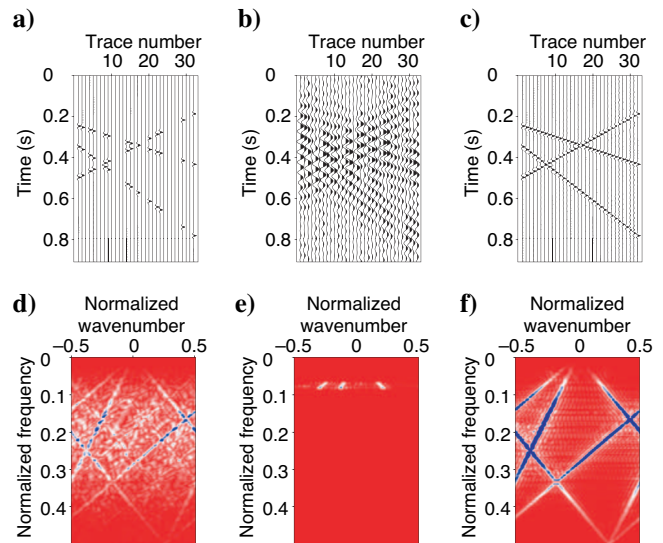


Figure 6. A synthetic example with three linear events. (a) Data with missing traces. (b) Reconstructed data using MWNI. (c) Reconstructed section using MWNI and MSAR with extrapolation of prediction filters to avoid gaps in Figure 7. (d) The f - k domain of (a). (e) The f - k domain of (b). (f) The f - k domain of (c).

in this example is very unlikely to happen. However, we must stress that the combination of MSAR and Spitz's extrapolation technique does provide a solution to this problem. In addition, it is important to mention that the low-frequency end of the data f_{min_r} could be high enough to yield this situation if aggressive low-pass filtering was used, for instance, to suppress ground roll.

Real data example

To test the performance of the MSAR reconstruction on a real data set, we apply the technique to the reconstruction of a near-offset section from a marine data set from the Gulf of Mexico. Events arising from diffractions on a salt body make the reconstruction difficult for the MWNI method. About 40% of the traces were removed from the original section (Figure 8a) to simulate a section with missing traces

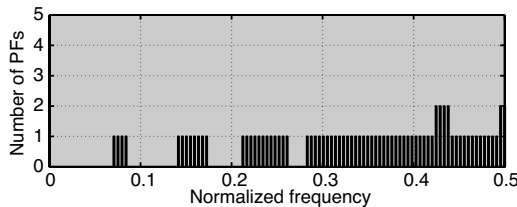


Figure 7. The number of prediction filters contributing to each frequency component in Figure 6c.

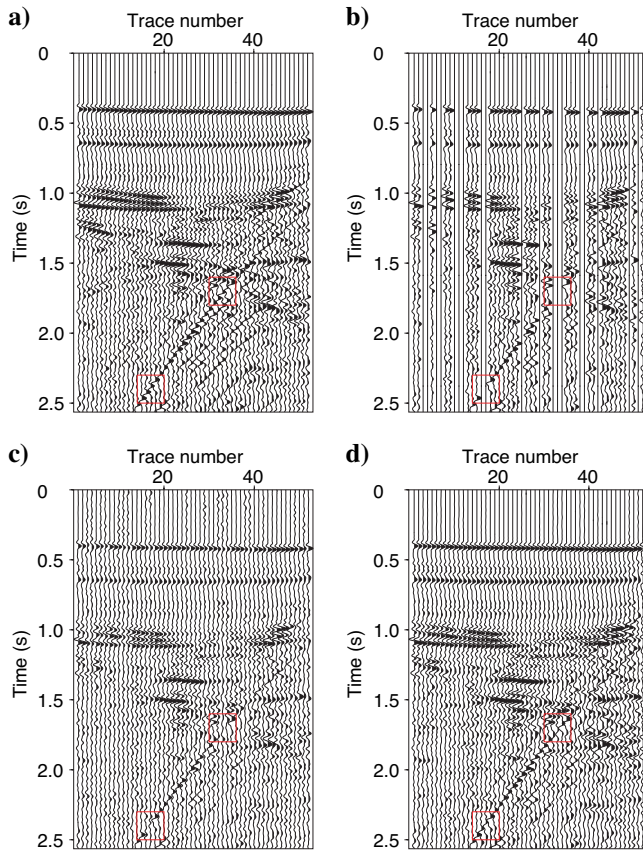


Figure 8. Reconstruction of a near-offset section. (a) Original section. (b) Section with missing traces. (c) Reconstructed section using MWNI. (d) Reconstructed section using MSAR. Regions indicated by red squares show the advantages of using MSAR.

(Figure 8b). The section of missing traces is reconstructed using MWNI (Figure 8c) and MSAR (Figure 8d). For this particular test, the length of the prediction filters is set to $L = 4$. From a comparison of these figures (notice in particular the areas indicated by red squares), it is easy to see that the combined application of MWNI and MSAR produces a result where the steeply dipping events are better preserved after reconstruction. In addition, Figure 9 shows the f - k representation of the data in Figure 8.

The f - k domain representation shows that the aliased event is preserved when MSAR is used to reconstruct the high frequencies (Figure 9d). The MSAR method is based on AR modeling of events in the f - x domain. In other words, MSAR can optimally model linear events in the t - x domain (complex sinusoids in f - x). The aforementioned assumption can be validated by applying MSAR in small spatio-temporal windows where curved events will appear as linear events. One must realize, however, that the scarcity of data in small windows can lead to suboptimal reconstructions.

Figure 10 shows the part of data reconstructed using MWNI. Figure 11 portrays the number of prediction filters contributing to the reconstruction of each frequency. It must be noted that because there was no signal at normalized frequencies larger than 0.22, the MSAR reconstruction was only performed for the normalized frequencies smaller than 0.22.

It should be noticed that we have not yet removed the alias from the data. At this stage, we have reconstructed the data (obtained the missing traces). An interpolation technique for regularly sampled data can now be used to de-alias the reconstructed data. Figure 12a

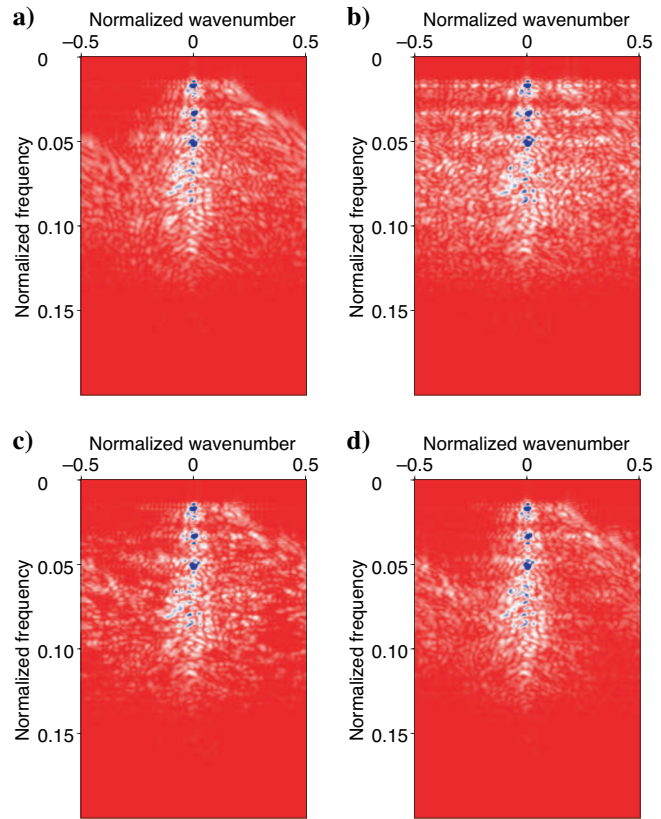


Figure 9. The f - k domain representation of Figure 8. (a) Original data. (b) The section of missing traces. (c) Reconstructed section using MWNI. (d) Reconstructed section using MWNI and MSAR.

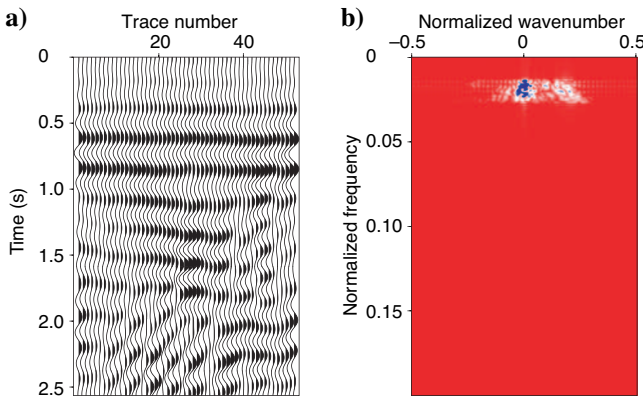


Figure 10. The reconstructed part of data using MWNI used to compute prediction filters for Figure 8d. (a) The data in t - x domain. (b) The data in f - k domain.

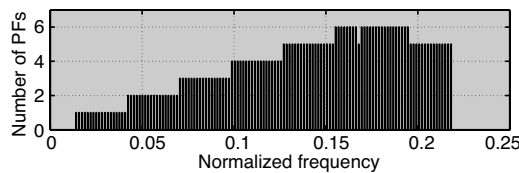


Figure 11. The number of prediction filters contributing to each frequency in the reconstruction portrayed in Figure 8d.

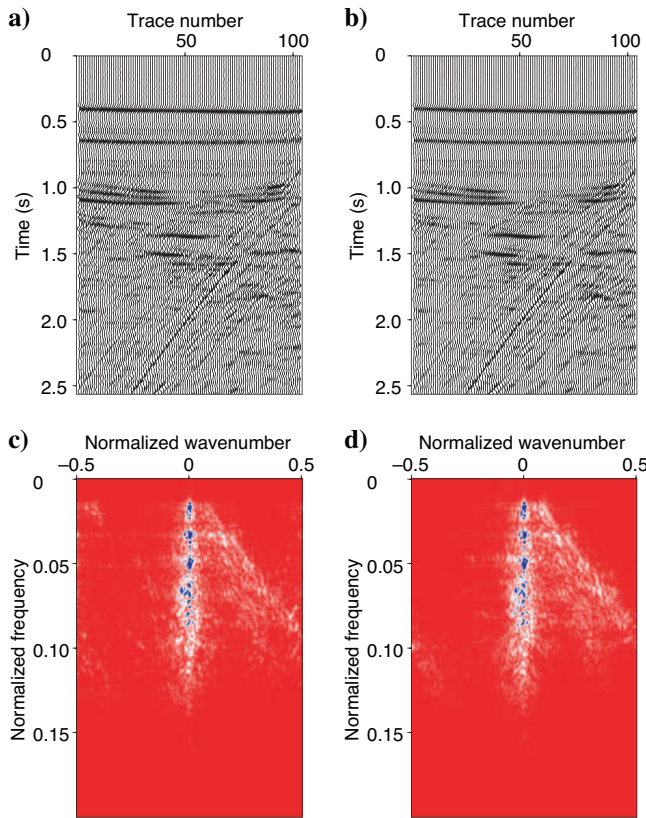


Figure 12. First-order interpolation of the final reconstructed section in Figure 8d. (a) Gulunay's f - k interpolation. (b) MSAR method. (c) f - k panel of a. (d) f - k panel of b.

and b show the result of first-order interpolation of the final reconstructed section (Figure 8d) using Gulunay's f - k interpolation method (Gulunay, 2003) and MSAR, respectively. In the MSAR de-aliasing case, we have considered that every second trace is missing. Figure 12c and d show the f - k representation of the Figure 12a and b, respectively. The aliasing of the diffraction event is removed to a high extent. Gulunay's interpolation shows some low-frequency artifacts which could be a by-product of the mask required by the method to annihilate the aliased part of the signals. In our implementation, MSAR de-alias uses the average of prediction filters. This is the main difference with Spitz (1991) where only one prediction filter for each frequency component is utilized.

DISCUSSION

The MSAR method could have potential problems in finding the required low-frequency components needed to extract the prediction filter associated to the reconstruction of a given high-frequency component. In this case, one can alleviate the problem by zero padding the data before applying the DFT. This reduces the frequency sampling interval; therefore, making it easier for the algorithm to find the required low frequencies. Alternatively, one can use the wrapped discrete Fourier transform (WDFT) to densely sample some specific band of frequencies (Makur and Mitra, 2001; Franz et al., 2003).

It is clear that any method based on the assumption of linear events will have problems at the time of modeling events with curvature. This facet does not escape our technique. In fact, departure from the linear-event model will introduce nonstationarity in the prediction problem and, consequently, the multistep algorithm will produce different prediction filters at each step. Claerbout and Fomel (2006) discusses this problem using expanding antialias operators in the t - x domain. As it has been mentioned by Spitz (1991), one can use small windows as a mean to validate the assumption of linear events. It is well-known that in most geophysical problems there is no free lunch; to solve a problem we require assumptions, in general these assumptions have to be partially violated to process real data. A good interpolation method should be robust when the assumption under which it was designed are not completely honored. Our algorithm is a good example of the latter; it can tolerate mild curvature in the waveforms, as portrayed by our real data examples.

Modifying MSAR for multidimensional data reconstruction is straightforward. In higher dimensions, the reconstruction of low frequencies using MWNI should be more stable, and as a result, the prediction filters can be calculated with high precision, leading to a better reconstruction of high frequencies. Spitz (1990) and Wang (2002) introduced a way to use 2D AR operators to interpolate the regularly sampled data in the f - x - y domain. The same style of AR operators can be used to extend the MSAR method to the 2D case.

CONCLUSIONS

In this paper, a method for spatial reconstruction of high-frequency data components was introduced. The method entails the cooperative application of a Fourier-based technique, MWNI, to reconstruct the unaliased part of the data and a MSAR algorithm to reconstruct the high-frequency, and potentially aliased, part of the data. The MSAR algorithm relies on extracting information from low frequencies (reconstructed via MWNI) to reconstruct high frequencies. Because the prediction filter of a given high frequency can be com-

puted from more than one reconstructed low frequency, more than one prediction filter can be extracted for a given high frequency. In this case, an average of prediction filters is used to reconstruct the data. This averaging scheme helps eliminate any potential noise contamination from corrupted frequency components.

The results of synthetic data reconstruction, and also the real data example, show that MSAR is capable of eliminating high-frequency artifacts often encountered when MWNI is used to reconstruct the complete seismic band. MSAR can be applied to regularly sampled sections as well. A real data example of interpolation of a regularly sampled section shows that MSAR can effectively be adopted to dealias seismic data.

ACKNOWLEDGMENTS

We acknowledge the financial support of the sponsors of the Signal Analysis and Imaging Group at the University of Alberta. We also thank the associate editor of GEOPHYSICS and the three reviewers for their valuable suggestions.

APPENDIX A

MINIMUM-WEIGHTED NORM INTERPOLATION (MWNI)

Interpolation of band-limited data with missing samples can be summarized in the following inversion scheme:

$$\text{Minimize } \|\mathbf{x}\|_{\mathcal{W}}^2 \text{ Subject to } \mathbf{Gx} = \mathbf{y} \quad (\text{A-1})$$

where $\|\cdot\|_{\mathcal{W}}$ indicates a specific weighted norm and \mathbf{G} is the sampling matrix which maps desired data samples \mathbf{x} to available samples \mathbf{y} . Its transpose, \mathbf{G}^T , fills the position of missing samples with zeros. A regularization norm can be selected in the wavenumber domain as follows:

$$\|\mathbf{x}\|_{\mathcal{W}}^2 = \sum_{k \in \mathcal{K}} \frac{X_k^* X_k}{W_k^2}, \quad (\text{A-2})$$

where X_k indicates the coefficients of the Fourier transform of the vector of spatial data \mathbf{x} . The values of W_k determine the type of interpolation. For band-limited MWNI a diagonal matrix is defined as:

$$\mathbf{Y}_k = \begin{cases} W_k^2 & k \in \mathcal{K} \\ 0 & k \notin \mathcal{K} \end{cases}, \quad (\text{A-3})$$

where \mathcal{K} indicates the region of support of the Fourier transform. The pseudoinverse of \mathbf{Y} is defined as:

$$\mathbf{Y}_k^\dagger = \begin{cases} W_k^{-2} & k \in \mathcal{K}, \\ 0 & k \notin \mathcal{K}. \end{cases} \quad (\text{A-4})$$

For band-limited minimum norm interpolation, the values of W_k are equal to one, although for MWNI, their values must be iteratively updated to find an optimal reconstruction. The minimizer of the cost function A-1 is given by

$$\hat{\mathbf{x}} = \mathbf{F}^H \mathbf{Y} \mathbf{F} \mathbf{G}^T (\mathbf{G} \mathbf{F}^H \mathbf{Y} \mathbf{F} \mathbf{G}^T + \alpha \mathbf{I})^{-1} \mathbf{y} \quad (\text{A-5})$$

where \mathbf{F} is the Fourier matrix, α is trade-off parameter, \mathbf{I} is the identity matrix, and T and H stand for transpose and Hermitian transpose

operators, respectively. For further details see Liu (2004) and Liu and Sacchi (2004).

APPENDIX B

MULTISTEP AUTOREGRESSIVE OPERATOR

In this appendix we provide a proof for the MSAR theory. A seismic section with linear events can be represented in the f - x domain as:

$$S(m\Delta x, n\Delta f) = \sum_{k=1}^L A_k e^{-i2\pi(n\Delta f)(m\Delta x)p_k}, \quad (\text{B-1})$$

where Δf and Δx are frequency and spatial sampling intervals, respectively. In addition, p_k and A_k are the slope and amplitude of each linear event, respectively. This means that each linear event, for a monochromatic frequency component f , can be represented as complex harmonic in the f - x domain. Now consider the case with $\Delta x' = \alpha \Delta x$ and $\Delta f' = \Delta f / \alpha$. In this case it is easy to show that

$$S(m\Delta x', n\Delta f') = S(m\alpha \Delta x, n\frac{\Delta f}{\alpha}) = S(m\Delta x, n\Delta f). \quad (\text{B-2})$$

In addition, one can show that a superposition of L harmonics can be represented by an AR model of the form:

$$S(m\Delta x, n\Delta f) = \sum_{j=1}^L P(j, n\Delta f) S((m-j)\Delta x, n\Delta f). \quad (\text{B-3})$$

Similarly if we use $\Delta f'$ and $\Delta x'$, we obtain:

$$S(m\Delta x', n\Delta f') = \sum_{j=1}^L P'(j, n\frac{\Delta f}{\alpha}) S((m-j)\alpha \Delta x, n\frac{\Delta f}{\alpha}). \quad (\text{B-4})$$

A comparison of equations B-2, B-5, and B-4 leads to the following expression

$$P'(j, n\frac{\Delta f}{\alpha}) = P(j, n\Delta f), \quad j = 1, 2, \dots, L \quad (\text{B-5})$$

which is the basis for the MSAR reconstruction method. Interested readers can find the basic definition and properties of prediction filters in Spitz (1991).

It can also be shown that there exist predictability properties for each component of the prediction filter on the frequency axis. This means that if the prediction filters are known for some frequencies, one can find the prediction filter for other frequencies by applying prediction operators to the prediction filter components. More succinctly, one can find the prediction filters of prediction filters. For further details see Spitz (1991, Appendix B).

REFERENCES

- Claerbout, J. F., and S. Fomel, 2006, Image estimation by examples, accessed April 2007; http://sepwww.stanford.edu/sep/prof/gee/lal/paper_html/node1.html.
- Duijndam, A., M. Schonewille, and C. Hindriks, 1999, Reconstruction of band-limited signals, irregularly sampled along one spatial direction: Geophysics, **64**, 524–538.

- Franz, S., S. K. Mitra, and G. Doblinger, 2003, Frequency estimation using warped discrete Fourier transform: *Signal Processing*, **83**, 1661–1671.
- Gulunay, N., 2003, Seismic trace interpolation in the Fourier transform domain: *Geophysics*, **68**, 355–369.
- Liu, B., 2004, Multi-dimensional reconstruction of seismic data: Ph.D. thesis, University of Alberta.
- Liu, B., and M. D. Sacchi, 2004, Minimum weighted norm interpolation of seismic records: *Geophysics*, **69**, 1560–1568.
- Liu, B., M. D. Sacchi, and D. Trad, 2004, Simultaneous interpolation of 4 spatial dimensions: 74th Annual International Meeting, SEG, Expanded Abstracts, 2009–2012.
- Makur, A., and S. K. Mitra, 2001, Warped Discrete-Fourier Transform: Theory and applications: *IEEE Transactions on Circuits and Systems I: Fundamental Theory and Applications*, **48**, 1086–1093.
- Porsani, M., 1999, Seismic trace interpolation using half-step prediction filters: *Geophysics*, **64**, 1461–1467.
- Sacchi, M., and B. Liu, 2005, Minimum weighted norm wavefield reconstruction for AVA imaging: *Geophysical Prospecting*, **53**, 787–801.
- Sacchi, M. D., T. J. Ulrych, and C. J. Walker, 1998, Interpolation and extrapolation using a high-resolution discrete Fourier transform: *IEEE Transaction on Signal Processing*, **46**, 31–38.
- Schonewille, M., R. Romijn, A. Duijndam, and L. Ongkiehong, 2003, A general reconstruction scheme for dominant azimuth 3D seismic data: *Geophysics*, **68**, 2092–2105.
- Spitz, S., 1990, 3-D seismic interpolation in the F-XY domain: 60th Annual International Meeting, SEG, Expanded Abstracts, 1641–1643.
- , 1991, Seismic trace interpolation in the f - x domain: *Geophysics*, **56**, 785–796.
- Wang, Y., 2002, Seismic trace interpolation in the f - x - y domain: *Geophysics*, **67**, 1232–1239.
- Wiggins, R., and S. Miller, 1972, New noise-reduction technique applied to long-period oscillations from the Alaska earthquake: *Bulletin of the Seismological Society of America*, **62**, 471–479.
- Zwartjes, P., and A. Gisolf, 2006, Fourier reconstruction of marine-streamer data in four spatial coordinates: *Geophysics*, **71**, no. 6, V171–V186.
- Zwartjes, P., and M. D. Sacchi, 2007, Fourier reconstruction of nonuniformly sampled, aliased seismic data: *Geophysics*, **72**, no. 1, V21–V32.